JTTEE5 24:1520–1528
DOI: 10.1007/s11666-015-0344-x
1059-9630/$19.00 © ASM International

Evaluation of Titanium Nitride-Modified Bondcoat System Used in Thermal Barrier Coating in Corrosive Salts Environment at High Temperature

Imran Nazir Qureshi, Muhammad Shahid, A. Nusair Khan, and Yaseer A. Durrani

(Submitted June 18, 2015; in revised form October 20, 2015)

Thermal barrier coating (TBC) systems were produced by air plasma spraying system on nickel base superalloy. These coatings were composed of a Y_2O_3-stabilized ZrO_2 topcoat and a CoNiCrAlY bondcoat and are known as standard TBC. In this paper, standard TBC samples were compared with TiN-modified bondcoat TBC samples. Titanium nitride was deposited by utilizing a physical vapor deposition technique. Both TBC systems were exposed to high temperature in the presence of corrosive salts, i.e. a mixture of V_2O_5 and Na_2SO_4 (50:50) for 50 h. It was observed that the TiN-modified samples showed better results in terms of oxidation resistance and delamination. The formation of $Cr_2Ti_{n-2}O_{2n-1}$ phases at the interface of the topcoat–bondcoat, in TiN-modified samples were found to enhance the thermal and oxidation properties of the TBC.

Keywords bondcoat modification, hot corrosion, thermal barrier coating, titanium nitride

1. Introduction

Thermal barrier coating (TBC) systems are being used to provide thermal insulation to hot sections of gas turbines to increase operating temperatures with better efficiency (Ref 1-7). The typical TBCs consist of a duplex structure comprised of a metallic bondcoat and a ceramic topcoat. Yttria-stabilized zirconia (YSZ) has been usually chosen for the top insulating coat material because of its low thermal conductivity and high coefficient of thermal expansion (10.7×10^{-6}/K) (Ref 8), which closely matches that of the Ni-based substrate (12.6×10^{-6}/K) (Ref 9). The small mismatch in the coefficient of thermal expansion (CTE) is further decreased by incorporation of the bondcoat (MCrAlY), which also improves adhesion. Moreover, the bondcoat also provides protection against oxidation and hot corrosion (Ref 10, 11). Recent results showed that MCrAlY having (wt.%) 22% cobalt (Co), 12% aluminium (Al), 18% chromium (Cr), and 0.5% yttrium (Y) and balance nickel (Ni) is a very successful material for the bondcoat (Ref 12-22). A third layer present in a TBC between the topcoat and the bondcoat is the thermally grown oxide (TGO) which forms during TBC deposition and its thickness increases during normal operation by diffusion of oxygen through the TBC (Ref 4, 5). It acts as diffusion barrier and reduces the speed of reaction between oxygen and elements such as Cr and Al present in the bondcoat. The α-Al_2O_3 oxide is the most preferable phase component of this layer in order to protect against oxidation above 900 °C (Ref 7). The thickness of the TGO increases during the oxidation process and is accompanied by stress at the interface of the bondcoat and the topcoat. Sometimes, this stress is more than the tolerance of the TBC, resulting in delamination of the coating at the interface. The life of the bondcoat is further limited due to oxidation/corrosion and interdiffusion between the substrate and the bond coatings.

MCrAlY coatings have been studied extensively for the last two decades (Ref 18-21). Significant amounts of work were carried out in developing the hot corrosion resistance of MCrAlY bond coatings which occurs due to the use of low-quality fuel containing impurities like sodium and vanadium (Ref 13-28). In the present investigation, an attempt has been made to enhance the life of TBCs by applying a thin layer of TiN on the bondcoat to improve its oxidation and hot corrosion resistance.

2. Experimental

The material of the substrates used in the experiments was Inconel-X750 (wt.%: Ni = 73, Cr = 15.5, Fe = 7, Ti = 2.5, Al = 0.7, C = 0.04) with dimensions of $25 \times 25 \times 2$ mm. The samples were cut from a sheet and

Imran Nazir Qureshi and **Muhammad Shahid**, School of Chemical and Materials Engineering, National University of Sciences and Technology, Islamabad, Pakistan; **A. Nusair Khan**, Institute of Industrial and Control System, Rawalpindi, Pakistan; and **Yaseer A. Durrani**, University of Engineering and Technology, Taxila, Pakistan. Contact e-mail: imrannazir@scme.nust.edu.pk.

the edges were tapered in order to avoid delamination of the coatings during the spraying process. The samples were thoroughly cleaned with acetone and placed in a circular fixture for sand blasting and plasma spraying. During sand blasting, the samples were bombarded with alumina sand at an angle of 90° to the surface to achieve a surface roughness (Ra) in the range of 3–3.5 μm. The fresh sand-blasted samples were cleaned with compressed air so that no residual sand particles were left on the metal surface.

The freshly blasted surfaces were immediately held in a chuck which was later rotated at an optimized speed of 120 rpm. For plasma spraying, a 9 MB Sulzer Metco gun was selected to deposit both the top- and bondcoats. The spraying gun was adjusted at a 90° angle to the substrates. In order to get a uniform thickness, the gun was moved to and fro relative to the rotating samples. The substrate temperature was maintained at ~170 °C using a constant flow of compressed air during the coating process. In this regard, an IR-camera was also installed at a distance of 4 m to monitor the temperature of the coatings. The distance between the substrate holder and the compressed air was maintained at 110 mm, to ensure the reproducibility of the coatings. All the important spraying parameters both for the topcoat and the bondcoat are shown in Table 1. All the samples were preheated so that no moisture was left on the surface before depositing the spraying powder, utilizing the same plasma gun. For the topcoat and the bondcoat, Metco-204B and AMDRY-995C powders were used, respectively. Details of the powders are given in Table 2. After the deposition of the bondcoat, the samples were removed from the fixture and a thin layer of TiN was deposited by a physical vapor deposition method. Finally, the topcoat was applied by air plasma spraying.

For the hot corrosion test, V_2O_5 and Na_2SO_4 were mixed in a ball mill in a 1:1 ratio (by weight). The mixture was spread over the as-sprayed samples with a concentration of 30 mg/cm^2, leaving a 3-mm surface/space from the edges free of salt to avoid an edge effect as per the procedure mentioned by Chen et al. (Ref 25). The melting points of Na_2SO_4 and V_2O_5 are 884 and 690 °C, respectively (Ref 26). The samples were placed in a stainless steel tray before loading into a furnace (Fig. 1). The samples were heated up to 950 °C, at the rate of 20 °C/min. The hot corrosion tests were run in cycles, each of 10 h duration. After each heating cycle, the furnace was shut down to let the samples cool to room temperature. They were then visually inspected before being subjected to the next heating cycle. A total of 5 such cycles (50 h) were given to the samples before conducting the results.

In order to confirm the formation of different phases in the TiN-modified samples after 50 h exposure, the topcoat was delaminated by a chemical etching process using 50% diluted HCl at room temperature. The chemical attacked the interface of both the bondcoat–topcoat and the substrate–bondcoat. Due to the relatively porous nature of the bondcoat, as compared to the substrate, the chemical preferentially dissolved the bondcoat. As a result, a delaminated topcoat was obtained with attached phases, formed during the hot corrosion. The delaminated topcoat was washed with water and preserved for further study.

Table 1 Plasma spraying parameters used to deposit coatings

Parameters	Spraying powder	
	CoNiCrAlY	YSZ
Current, A	600	600
Voltage, V	66	66
Primary gas, Ar (SLPM)	55	32
Secondary gas, H_2 (SLPM)	8	10
Powder feed rate, g/min	150	150
Spray distance, mm	110	110

3. Results and Discussion

3.1 Surface of Topcoat After Hot Corrosion

A little spalling was observed at the edges of the topcoat in both types of samples after 10 h exposure. These edges were probably spalled under the thermal stress due to the first time direct charging of the samples at high temperature. After 30 h of exposure, it was revealed that the standard samples spalled more than the TiN-modified

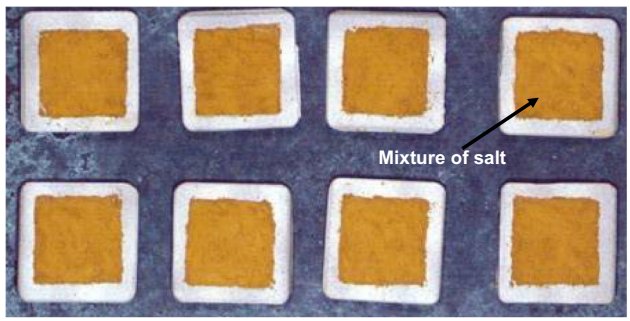

Fig. 1 Standard TBC samples (upper) and TiN modified sample (lower), placed in a stainless steel plate, with salt mixture on the top surface of the samples

Table 2 Chemical compositions (wt.%), particle size range and morphology of the spraying powders used to deposit the coatings

Powder	Chemistry	Particle size range, μm	Particle morphology
Metco-204B (topcoat)	Zirconia stabilized with 8% yttria	45–75	Spherical
AMDRY-955C (bondcoat)	Co32-Ni21-Cr8-Al0.5-Y	45–75	Spherical

samples (Fig. 2. After the exposure of 50 h, the standard samples showed about 10–12% spalling, whereas the TiN-modified samples spalled only a little at the edges (Fig. 2).

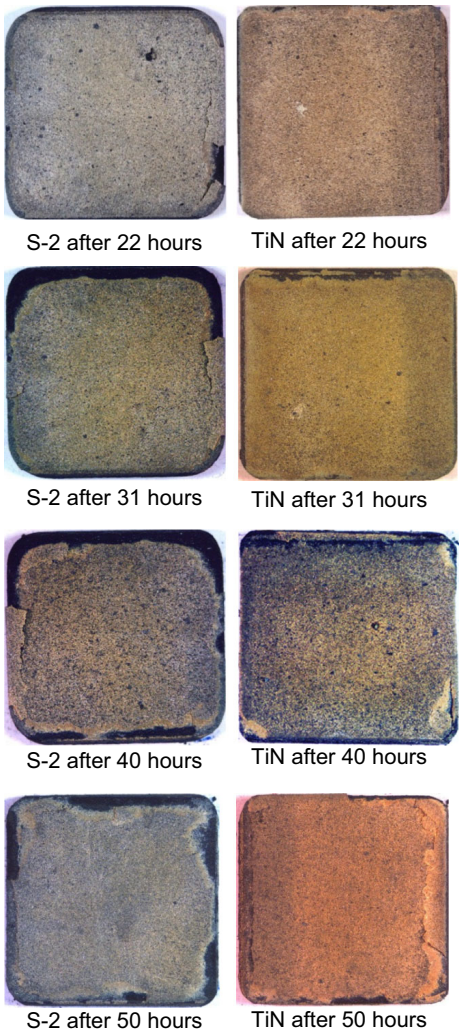

Fig. 2 *S-2* (standard TBC) and *TiN*-modified samples showing the condition of the top surfaces after different time intervals, treated at 950 °C in a hot corrosion environment

High-magnification images of the topcoat of the two systems revealed the rods of YVO_4 (yttrium vanadate). In both cases, the rods were randomly dispersed on the surface of the topcoat (Fig. 3). It appears that the salt mixture reacted and formed a eutectic compound, $NaVO_3$:

$$Na_2SO_4 + V_2O_5 \rightarrow 2\ NaVO_3 + SO_2 + 1/2O_2. \quad \text{(Eq 1)}$$

The $NaVO_3$ compound acted as an oxygen carrier and entered into the pores of the plasma-sprayed topcoat. It reacted with the Y_2O_3 (present in the solid solution of Y_2O_3-stabilized ZrO_2) forming YVO_4 as per following the reaction (Ref 27):

$$ZrO_2(Y_2O_3) + 2NaVO_3 \rightarrow ZrO_2 + 2YVO_4 + Na_2O. \quad \text{(Eq 2)}$$

The loose powder, which was found as debris on the topcoat surface, was analyzed as ZrO_2 which was left after the formation of the YVO_4 rods.

3.2 Microstructural Analysis

3.2.1 Cross-section of As-Sprayed Coatings. The cross-section of the two systems demonstrated typical air plasma-sprayed coating features, i.e. micro-cracks, lamella of semi-molten particles and shrinkage cavities. It was estimated that about 8–12% pores were present in the topcoat. A typical lamellar structure was observed predominantly in the bondcoat after the air plasma spraying process (Fig. 4).

It was noted that the thickness of the TiN deposited on the bondcoat varied from 6 to 10 μm (Fig. 5). It was found that the sputtered layer was not deposited properly at some locations (Fig. 5). Furthermore, a few vertical cracks were also observed within the TiN thin layer (Fig. 5). This cracking may be due to stress relaxation of the coating during pre-heating before the deposition of the topcoat.

3.2.2 Cross-section After Hot Corrosion. The TiN-modified samples, after 50 h of hot corrosion testing, demonstrated that the overall oxidation condition of the bondcoat is less severe as compared to the standard samples (Fig. 6). This confirms that TiN acted as a good barrier against oxygen at high temperature. It was observed that the TiN-modified system had formed a denser and uniformly thick oxides layer at the topcoat–bondcoat interface (Fig. 7) However, in the case of the standard

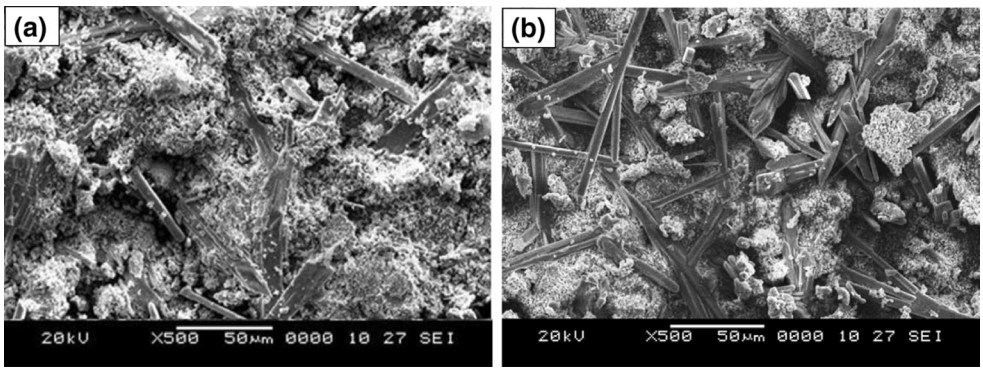

Fig. 3 Top surfaces of the standard TBC (a) and the TiN-modified sample (b) showing rod-like features after 50 h exposure

system, the oxide layer was irregular and scattered within the bondcoat and topcoat (Fig. 8) The inherent defects of plasma-sprayed coatings such as porosity and splat boundaries acted as diffusion channels for corrosive liquids. EDS analysis of the bondcoat showed that no ''vanadium'' was present in the TiN-modified samples, whereas the bondcoat of the standard samples revealed ''vanadium'' in the analysis (Fig. 9). This demonstrates that vanadium oxide crossed the diffusion barrier of alumina (TGO) in the case of the standard samples, whereas the TiN layer offered resistance against its penetration.

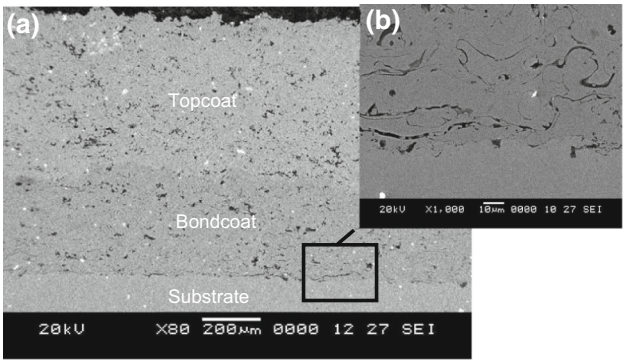

Fig. 4 (a) SEM micrograph showing typical structure of the as-sprayed TBC coating. (b) Lamellar structure in the bondcoat

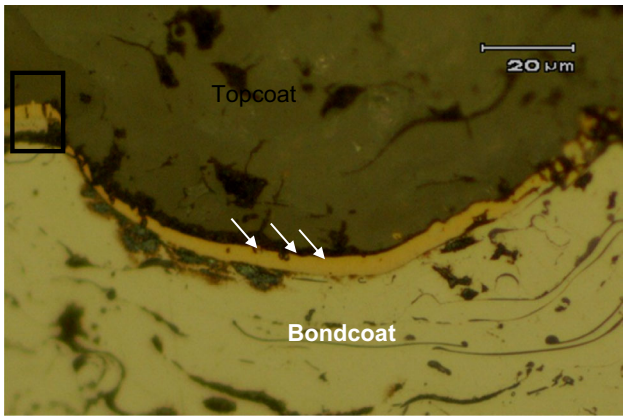

Fig. 5 Optical micrograph showing layer of TiN (arrows) and interface. Vertical cracks (box) are also present at some locations

At high magnification, the TiN-modified samples revealed different features at the bondcoat–topcoat interface. It was observed that, at high temperature, TiN destabilized and formed other compounds in the presence of abundant oxygen. TiN is not stable above 600 °C (Ref 28), and it seems that, above this temperature, TiN oxidized to Magneli phase Ti_nO_{2n-1} ($4 \leq n \leq 9$) (Ref 29) which had a complicated defect structure (Ref 30).The point defects present in these systems are dominated by oxygen vacancies and titanium interstitials (Ref 29, 31). The so-called Magneli phases have long order defect structures (Ref 29). These phases further react with chromium oxides and may form a series of homologous structures, i.e. $Cr_2Ti_{n-2}O_{2n-1}$ ($6 \leq n \leq 9$). The $Cr_2Ti_{n-2}O_{2n-1}$ phase is known from its stability against thermal stresses and oxidation (Ref 32).

EDS analysis, in atomic percentages, may give some idea of the atomic ratios in the compound. Thus, the most abundantly formed phase, present at the boundaries of the topcoat–bondcoat interface, revealed that the atomic ratio of Ti:Cr is 3. Figure 10 shows three different points from where the EDS analysis was taken. The at.% composition obtained from these points is shown in Table 3. These indicated that the $Cr_2Ti_5O_{13}$ phase is predominantly formed at the topcoat–bondcoat interface, after 50 h of exposure. $Cr_2Ti_5O_{13}$ is known as stable up to 1485 °C (Ref 33).

The formation of $Cr_2Ti_5O_{13}$ at the topcoat–bondcoat interface can be explained by two mechanisms. First, at high temperature, the destabilized TiN transformed to titanium oxide which further reacted with the underlying chromium of the bondcoat thus forming $Cr_2Ti_{n-2}O_{2n-1}$. The formation of these compounds by the same mechanism is supported by the work of Winde (Ref 34) in which the Cr films were deposited on the surface of the TiO_2 crystals and then the influence of temperature and surface stoichiometry was studied

$$Ti_nO_{2n-1} + Cr \rightarrow Cr_2Ti_{n-2}O_{2n-1}. \quad \text{(Eq 3)}$$

Another mechanism of formation of these types of compounds can be explained by the fact that some places were left uncoated during TiN deposition while the other sites demonstrated cracks within the TiN coating. These sites

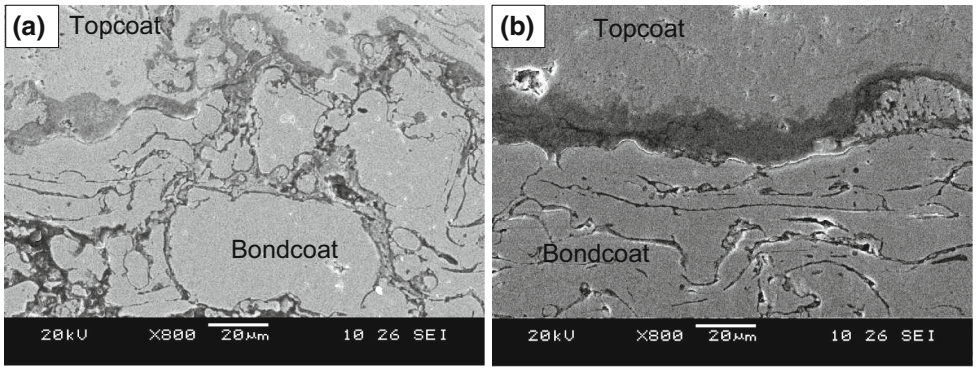

Fig. 6 Cross-section of both standard TBC (a) and TiN-modified (b) samples, after 50 h exposure in a hot corrosion environment

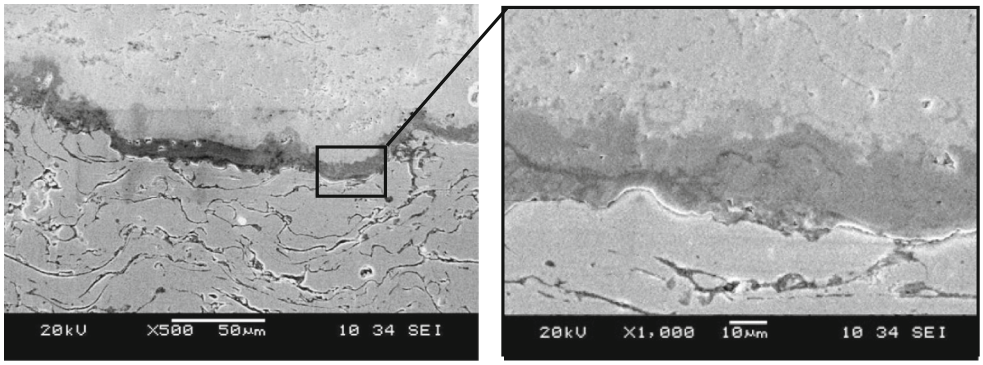

Fig. 7 Cross-section of the TiN-modified sample after 50 h exposure in a hot corrosion environment demonstrating a dense and uniform oxide layer at the bondcoat–topcoat interface

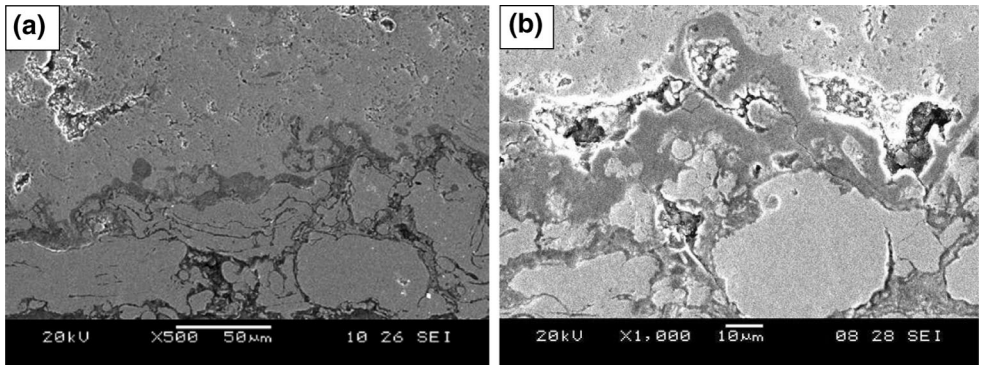

Fig. 8 Non-uniform oxide layer in the standard TBC sample after 50 h exposure: (a) low magnification, (b) high magnification

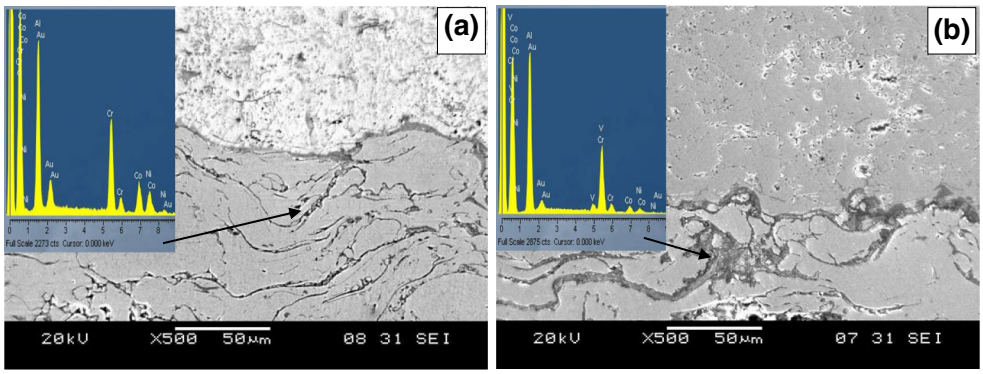

Fig. 9 EDS analysis at the boundaries of the splats in the bondcoat showing no ''vanadium'' was present in the TiN-modified samples (a), while the standard TBC samples demonstrated the presence of vanadium (b) near the topcoat–bondcoat interface

provided paths for oxygen and as a result the formation of alumina and chromium oxides took place at the topcoat–bondcoat interface. Thus, the other mechanism of the formation of $Cr_2Ti_{n-2}O_{2n-1}$ could be that the chromium oxides directly reacted with titanium oxides at high temperature.

$$Ti_nO_{2n-1} + Cr_2O_3 \rightarrow Cr_2Ti_{n-2}O_{2n-1}. \quad \text{(Eq 4)}$$

These types of reactions are also explained by other researchers like Somyia et al. (Ref 29) and Harju et al. (Ref 35).

In case of the standard bondcoat system, the oxides formation was rather different. It was observed that, after 50 h exposure at high temperature, spinels and pervoskite-type structures were formed. In this regard, aluminum and chromium oxides were formed first and then reacted with the oxides of Ni and Co forming $CoCr_2O_4$, $NiCr_2O_4$, $NiCrO_3$, $CoNiO_3$ and $NiCrO_4$ phases (Ref 27). These phases formed at the topcoat–bondcoat interface. The formation of some of the above-mentioned spinels and pervoskite structures in the standard bondcoat system are demonstrated in Fig. 11, whereas Table 4 shows the atomic percentage of these compounds.

3.2.3 Delaminated Topcoat Obtained after Hot Corrosion. The topcoat of the TiN modified sample which

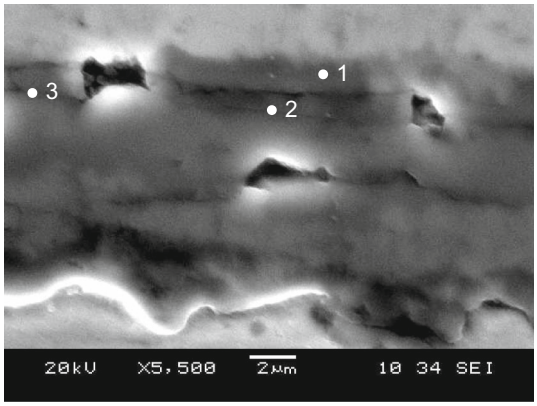

Fig. 10 Different sites are marked from where EDS analysis at the topcoat–bondcoat interface were taken in the TiN-modified sample after 50 h exposure. EDS analysis results are shown in Table 3

Table 3 Average chemical compositions (at.%) of various phases marked in Fig. 11 for the TiN-modified sample exposed for 50 h at 950 °C

Spectrum	Al	Ti	Cr	Fe	Co	Ni	Y	Zr
Spectrum 1	3.34	59.17	20.07	0.12	6.44	3.19	0.51	4.54
Spectrum 2	5.62	44.87	13.98	0.37	7.26	4.14	6.77	14.12
Spectrum 3	3.69	58.45	17.02	0.24	5.55	2.78	1.49	8.47

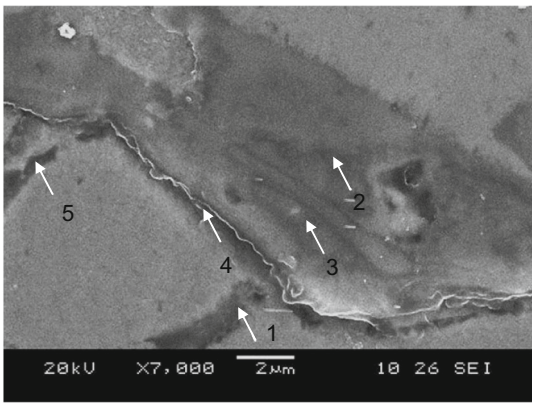

Fig. 11 Standard TBC sample (after 50 h exposure) demonstrating the topcoat–bondcoat interface. Sites *1–5* are shown from where the EDS analysis was taken and reported in Table 4

was subjected to hot corrosion test for 50 h was delaminated by chemical etching and observed in SEM. The light and dark grey regions were observed as attached to the topcoat. EDS observations revealed that these grey regions were rich in alumina and chromium oxides (Fig. 12). It seemed that the layers of alumina and chromium oxide were present on that side of topcoat which faced the

Table 4 Average chemical compositions (at.%) of various phases marked in Fig. 12 for the standard TBC sample exposed for 50 h at 950 °C

Age, at.%					
Location	Al	Cr	Co	Ni	Possible phase
1	8	19	36	37	$CoNiO_3$
2	43	36	10	10	$AlCrO_3$
3	39	45	9	7	
4	49	15	18	17	Al_2O_3
5	6	21	38	35	$CoNiO_3$

bondcoat. Further, investigation revealed that patches of chromium-titanium phases having distinct physical characteristics were also present. The chromium-titanium rich phase with crystals like structure was present closer to the topcoat surface (Fig. 13). Chemical composition, in at.%, analysis showed the similar composition as was determined in the cross-sections of the same samples (Fig. 10). This confirms the presence of a chromium-titanium phase with the Ti:Cr ratio in the range of 2.5–4, referring to the fact that $Cr_2Ti_{n-2}O_{2n-1}$ ($Cr_2Ti_6O_{15}$, $Cr_2Ti_5O_{13}$ and $Cr_2Ti_7O_{17}$) phases were formed.

3.3 X-ray Diffraction Analysis

3.3.1 As-Sprayed Topcoat. X-ray diffraction analysis of the as-sprayed TiN-modified samples along with standard samples was made. It was observed that a 100% tetragonal-ZrO_2 structure was formed after spraying. However, after 50 h, at high temperature in the hot corrosion environment, the presence of monoclinic-ZrO_2 phase along with yttrium vanadate (YVO_4) was observed. Vanadate salts attacked the Y_2O_3 present in the solid solution of ZrO_2, and thus destabilized the tetragonal-ZrO_2 (Fig. 14). The formation of a monoclinic phase is associated with volumetric changes (Ref 27) and thus leads to the delamination of the top surface.

3.3.2 Delaminated Coating of TiN-Modified Sample. The portion of the delaminated topcoat that faces the bondcoat (Fig. 13b) is important because diffusion and oxidation processes occurred through this interface during the hot corrosion. It is also important to investigate the reasons why the TiN-modified bondcoats demonstrated comparatively better results than the standard bondcoated samples. Further, it is necessary to confirm the EDS analysis (at.%) results showing the formation of the $Cr_2Ti_{n-2}O_{2n-1}$ phase, as discussed in the previous section.

In this regard, the grey surface (the portion next to the bondcoat) of the delaminated topcoat, obtained after chemical etching, was analyzed with XRD. The results demonstrated that, after 50 h at high temperature in the hot corrosion environment, different phases were formed at the topcoat–bondcoat interface. In these phases, alumina, chromium oxide (Cr_3O_4, Cr_2O_3) and the formation of $Cr_2Ti_5O_{13}$ were confirmed (Fig. 15).

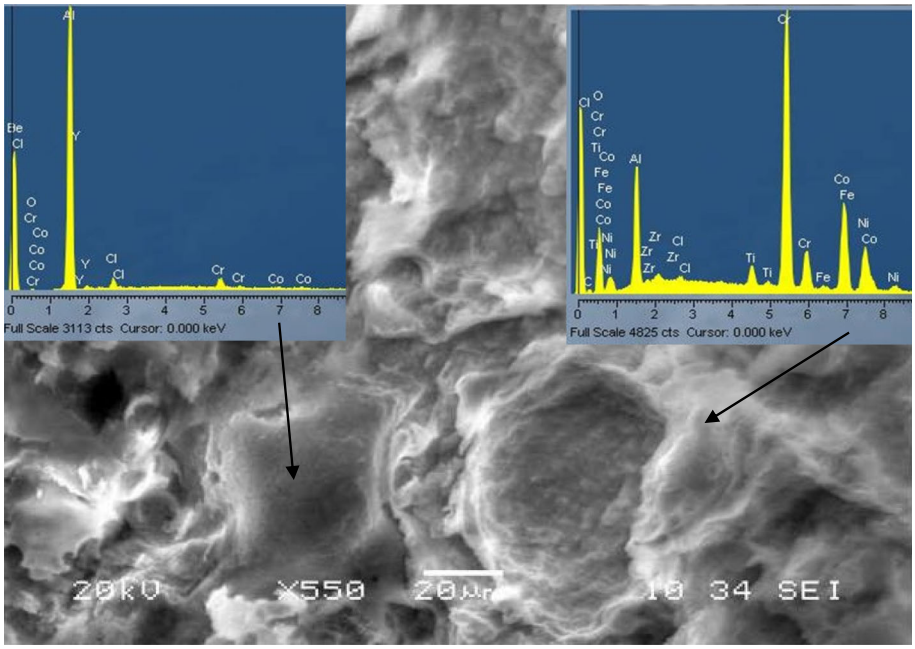

Fig. 12 Delaminated topcoat of the TiN-modified sample (after 50 h exposure) demonstrating the regions which were broken away from the bondcoat; two regions rich in alumina and chromium oxides

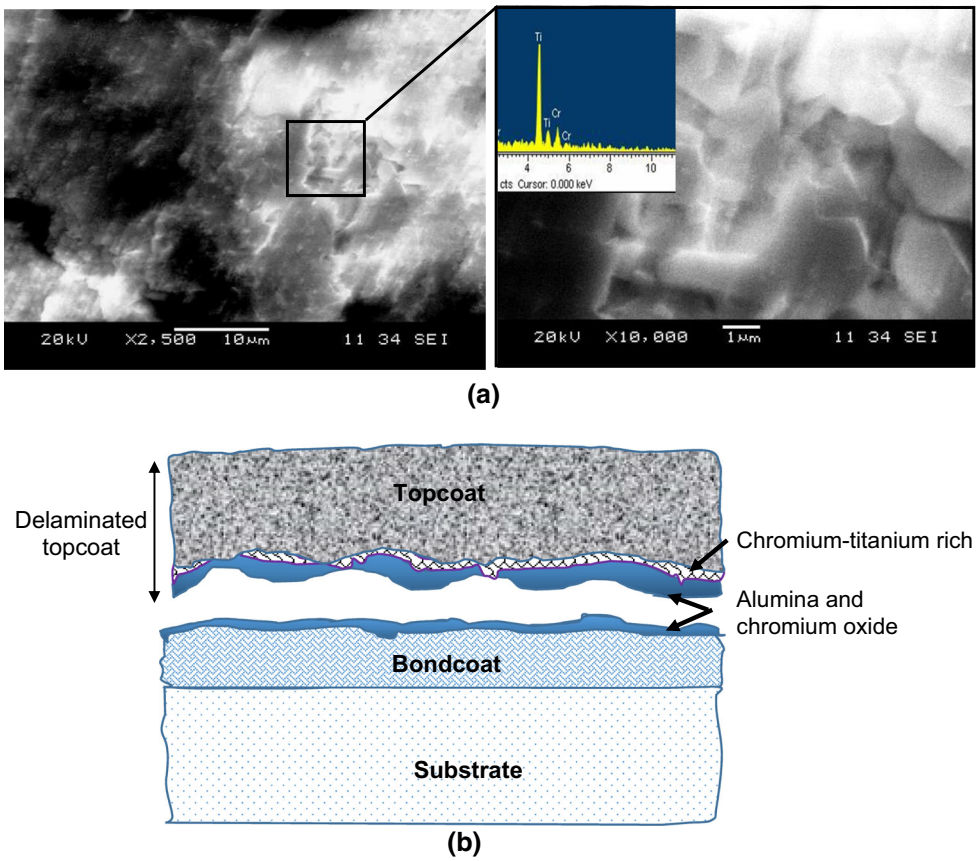

Fig. 13 (a) TiN-modified sample (after 50 h exposure) showing patches (box) of chromium-titanium phases having a crystal-like structure. (b) Schematic representation of delaminated topcoat showing layers of alumina and chromium oxide and layer with chromium-titanium phase

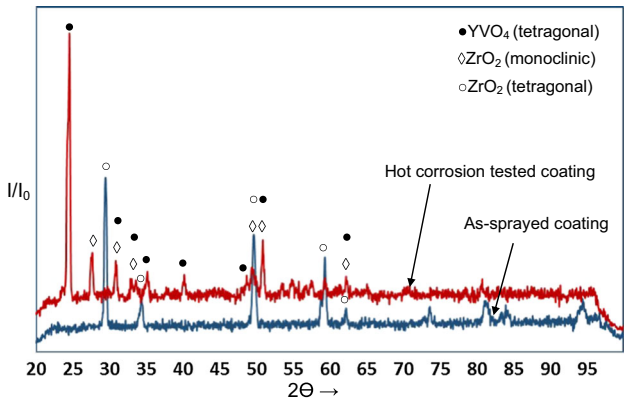

Fig. 14 XRD patterns comparing the scans of the as-sprayed coating with the sample exposed at 950 °C for 50 h

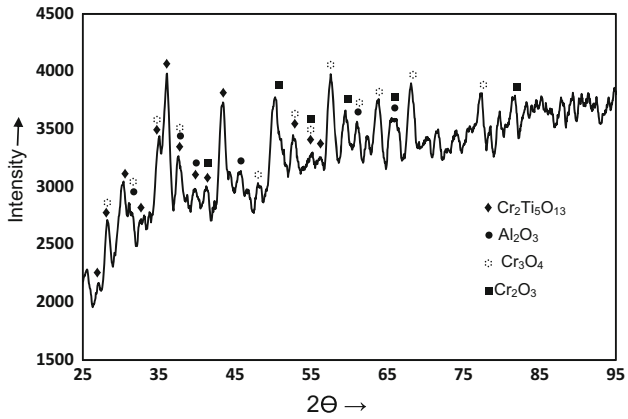

Fig. 15 XRD pattern showing different phases formed in the delaminated coating of the TiN-modified sample exposed at 950 °C for 50 h

4. Conclusion

It was demonstrated in this study that a TiN-modified bondcoat can enhance the oxidation properties of TBC systems in hot corrosion environments. This improvement is due to the formation of a $Cr_2Ti_{n-2}O_{2n-1}$ phase having good stability at high temperature against oxidation and delamination. In comparison to the above, standard TBC systems, i.e. without bondcoat modification, delaminated earlier due to the formation of spinels and perovskite structures.

References

1. A.G. Evans, D.R. Mumm, J.W. Hutchinson, G.H. Meier, and F.S. Pettit, Mechanisms Controlling the Durability of Thermal Barrier Coatings, *Prog. Mater. Sci.*, 2001, **46**, p 505
2. J.R. Brandon and R. Taylor, Microstructure, Composition and Property Relationships of Plasma-Sprayed Thermal Barrier Coatings, *Surf. Coat. Techol.*, 1992, **5**(2), p 141
3. I. Gurrappa, Thermal Barrier Coatings for Hot Corrosion Resistance of CM 247 LC Superalloy, *J. Mater. Sci. Lett.*, 1998, **17**, p 1267
4. R.L. Jones, Some Aspects of the Hot Corrosion of Thermal Barrier Coatings, *J. Therm. Spray Technol.*, 1997, **6**(1), p 77
5. B.A. Nagaraj and D.J. Wortman, Development of Corrosion Resistant Coatings for Marine Gas Turbine Applications, *Trans. ASME*, 1990, **112**, p 536
6. R. Srinivasan and J.M. Merrilea, The Hot Corrosion Resistance of 20 mol% $YTaO_4$ Stabilized Tetragonal Zirconia and 14 mol% Ta_2O_5 Stabilized Orthorhombic Zirconia for Thermal Barrier Coating Applications, *Surf. Coat. Technol.*, 2002, **160**, p 187
7. R.L. Jones, India as a Hot Corrosion-Resistant Stabilizer for Zirconia, *J. Am. Ceram. Soc.*, 1992, **75**(7), p 1818
8. X.Q. Cao, R. Vassen, and D. Stoever, Ceramic Material for Thermal Barrier Coatings, *J. Eur. Ceram. Soc.*, 2004, **24**, p p1-10
9. Inconal-X750 Data Sheet, The Special Metals Corporations, USA
10. A. Nusair Khan, J. Lu, and H. Liao, Effect of Residual Stresses on Air Plasma Sprayed Thermal Barrier Coatings, *Surf. Coat. Technol.*, 2003, **168**, p 291-299
11. H. Edris, D.G. McCartney, and A.J. Sturgeon, Microstructural Characterization of High Velocity Oxy-Fuel Sprayed Coatings of Inconel 625, *J. Mater. Sci.*, 1997, **32**, p 863-868
12. I. Gurrappa, Identification of Hot Corrosion Resistant MCrAlY Based Bond Coatings for Gas Turbine Engine Applications, *Surf. Coat. Technol.*, 2001, **139**, p 272
13. I. Gurrappa, Influence of Alloying Elements on Hot Corrosion of Superalloys and Coatings: Necessity of Smart Coatings for Gas Turbine Engines, *Mater. Sci. Technol.*, 2003, **9**, p 178
14. I. Gurrappa, Hot Corrosion Behavior of Nimonic-75, *J. High Temp. Mater. Sci.*, 1997, **38**, p 137
15. I. Gurrappa, Effect of Aluminum on Hot Corrosion Resistance of MCrAlY-Based Bond Coatings, *J. Mater. Sci. Lett.*, 2001, **20**, p 2225
16. I. Gurrappa, Overlay Coatings Degradation—An Electrochemical Approach, *J. Mater. Sci. Lett.*, 1999, **18**, p 1713
17. K.L. Luthra and D.A. Shores, Mechanism of Na_2SO_4 Induced Corrosion at 600-900 °C, *J. Electrochem. Soc.*, 1980, **127**, p 2202
18. C. Leyens, K. Fritscher, and M. Peters, Oxide Scale Formation on a MCrAlY Coating in Various H_2-H_2O Atmospheres, *Surf. Coat. Technol.*, 1996, **139**(1-2), p 133
19. W. Beele, N. Czech, W.J. Quadakkers, and W. Stamn, Long-Term Oxidation Tests on a Re-containing MCrAlY Coating, *Surf. Coat. Technol.*, 1997, **94-95**, p 41
20. A. Strawbridge, H.E. Evans, and C.B. Ponton, Spallation of Oxide Scales from NiCrAlY Overlay Coatings, *Mater. Sci. Forum*, 1997, **251-254**, p 365
21. C. Leyens, K. Fritcher, M. Peters, and W.A. Kayser, Transformation and Oxidation of a Sputtered Low-Expansion Ni-Cr-Al-Ti-Si Bond Coating for Thermal Barrier Systems, *Surf. Coat. Technol.*, 1997, **94-95**, p 155
22. S.R.J. Saunders and J.R. Nicholls, Hot Salt Corrosion Test Procedures and Coating Evaluation, *Thin Solid Films*, 1984, **119**(1), p 247
23. E. Erdos and A. Rehmel, Identification of the Spinel $(Cr, Al)_3S_4$ in the Internal Sulfidation Zone of Al-Diffusion Coatings, *Oxid. Met.*, 1986, **26**, p 101
24. E.Y. Lee, R.R. Biederman, and R.D. Sission, Jr., Diffusional Interactions and Reactions Between a Partially Stabilized Zirconia Thermal Barrier Coating and the NiCrAlY Bond Coat, *Mater. Sci. Eng.*, 1989, **120-121**, p 467
25. X. Yu, Y. Zhao, L. Gu, B. Zou, Y. Wang, and X. Cao, Hot Corrosion Behaviour of Plasma Sprayed YSZ/$LaMgAl_{11}O_{19}$ Composite Coatings in Molten Sulfate-Vanadate Salt, *Corros. Sci.*, 2011, **53**, p 2335-2343
26. A. Afrasiabi, M. Saremi, and A. Kobayashi, A Comparative Study on Hot Corrosion Resistance of Three Types of Thermal Barrier Coatings: YSZ, YSZ + Al_2O_3 and YSZ/Al_2O_3, *Mater. Sci. Eng.*, 2008, **478A**, p 264-269
27. C.S. Ramachandran, V. Balasubramanian, and P.V. Ananthapadmanabhan, On the Cyclic Hot Corrosion Behavior of Atmospheric Plasma Sprayed Lanthanum Zirconate Based Coatings in Contact with a Mixture of Sodium Sulphate and Vanadate Salts: A Comparison with the Traditional YSZ Duplex and NiCrAlY Coated Samples, *Vacuum*, 2013, **97**, p 81-95

28. E.A. Brandes and G.B. Brook, Eds, *Smithels Metals Reference Book*, 7th ed., Butterworth Heinemann, Oxford, 1999, p 27-24
29. L.A. Bursill and B.G. Hyde, Crystallographic Shear in the Higher Titanium Oxides: Structure, Texture, Mechanisms and Thermodynamics, *Prog. Solid State Chem.*, 1972, **7**, p 177
30. G.J. Woodand and L.A. Bursill, The Formation Energy of Crystallographic Shear Planes in Ti_nO_{2n-1}, *Proc. R. Soc. Lond.*, 1981, **A375**, p 105
31. E. Cho, S. Han, H.S. Ahn, K.R. Lee, S.K. Kim, and C.S. Hwang, First-Principles Study of Point Defects in Rutile TiO_{2-x}, *Phys. Rev. B*, 2006, **73**, p 193-202
32. J.P. Carmo and J.E. Ribeiro, Eds., *New Advances in Vehicular Technology and Automotive Engineering*, Croatia: In Tech, 2012, p 133
33. S. Somiya, S. Hirano, and S. Kamiya, Phase Relations of the Cr_2O_3-TiO_2 System, *J. Solid State Chem.*, 1978, **25**, p 273-284
34. C. Winde, Deposition and Characterization of Cr-Films on TiO_2 (110) Surfaces, Doctorate Dissertation, Max-Planck Institut für Metallforschung, Stuttgart, 2002
35. M. Harju, E. Levanen, and T. Mantyla, Wetting Behaviour of Plasma Sprayed Oxide Coatings, *Appl. Surf. Sci.*, 2006, **252**, p 8514-8520